Novel polymer electrolyte based on cob-web electrospun multi component polymer blend of polyacrylonitrile/poly(methyl methacrylate)/polystyrene for lithium ion batteries—Preparation and electrochemical characterization

Raghavan Prasanth[a], *Vanchiappan Aravindan*[b], *Madhavi Srinivasan*[a,b,*]

[a] *School of Materials Science and Engineering, Nanyang Technological University, Block N4.1, 50 Nanyang Avenue, Singapore 639798, Singapore*

[b] *Energy Research Institute @ NTU (ERI@N) Research Techno Plaza, 50 Nanyang Drive, Singapore 637553, Singapore*

** Corresponding author. Tel.: +65 67904606; fax: +65 67909081.*
E-mail address: madhavi@ntu.edu.sg (M. Srinivasan).

ABSTRACT

The aim of the present work is to prepare a novel polymer electrolyte (PE) based on multi component polymer blend of polyacrylonitrile (PAN), poly(methyl methacrylate) (PMMA) and polystyrene (PS) with varying compositions by electrospinning. Structural characterization is carried out using X-ray diffraction (XRD). The thermal and crystalline properties of the blend are studied by thermo-gravimetric analysis (TGA) and differential scanning calorimetry (DSC), respectively. Morphology of the membrane is examined by field emission scanning electron microscope (FE-SEM). The voids and cavities generated by the interlaying of the fibers are effectively utilized for the preparation of PE by loading with lithium hexafluorophosphate ($LiPF_6$) dissolved in ethylene carbonate (EC)/diethyl carbonate (DEC). The ionic conductivity of the polymer blend electrolyte is studied by varying the PMMA and PS content in the PAN matrix. The blend polymer electrolyte shows ionic conductivity of about 3.9×10^{-3} S cm^{-1}. The performance evaluation in coin cells show good charge–discharge properties and stable cycle performance under the test conditions. The result shows that the prepared polymer blend electrolytes are promising materials for lithium ion batteries.

Keywords

Polymer electrolytes; Lithium-ion batteries; Electrospinning; Polymer blend; Ionic conductivity

1. Introduction

Polymer electrolytes (PEs) composed of polymers singly or as blends complexed with suitable salts impart good safety characteristics to lithium ion batteries (LIBs). PEs are a relatively under explored part of modern batteries. Use of a PE to overcome safety problems associated with lithium batteries was proposed in the early 1980s. Solid polymer

electrolytes (SPEs) as well as gel polymer electrolytes (GPEs) were extensively reported by many groups [1–3]. All those PEs possessed very low room temperature ionic conductivity as compared to the aprotic organic electrolytes used in conventional lithium cells. Common GPEs exhibit high ionic conductivities (~10^{-3} S cm^{-1}) [4], however, their mechanical properties are not sufficient for practical applications. The recent attention to GPEs is thus focused on achieving high ionic conductivities as well as good mechanical properties. In connection with this, the novel preparation method of the PEs based on polymer blends or copolymers has been reported [5–7]. GPEs are prepared by immersing the porous polymer film in aprotic solvent with high dielectric constant, which dissolves enough charge carriers and provides more mobile medium for the ions, thereby enhancing the conductivity of the resultant films [5]. The conductivity of GPEs is dominated by quantity of the liquid electrolyte absorbed by the polymer matrix, porosity and pore distribution. It is important for good cell performance that the absorbed liquid electrolyte sustains within the polymer matrix during cycling.

In GPEs, the polymer component would render necessary stability to the lithium anode/electrolyte interface, which thereby reduces dendrite growth on lithium anode. GPEs, based on poly(vinylidene fluoride) (PVdF) [8], poly(vinylidene fluoride-*co*-hexafluoropropylene) {P(VdF-co-HFP)} [9], poly(methyl methacrylate) (PMMA) [10] and poly(acrylonitrile) (PAN) [11] have been widely studied as host polymers. The membrane properties such as porosity, tortuosity and uniformity of pore distribution are strongly dependent on its processing method. Different methods such as solvent casting [12], plasticizer extraction [13], phase inversion [14] and electrospinning [9] have been reported for the membrane preparation. Compared to cast membranes, it is reported that the GPE based on electrospun membranes shows higher porosity, electrolyte uptake and ionic conductivity due to the presence of fully interconnected pore structure [14]. Electrospinning is a simple and versatile method which is gaining importance in recent years as membranes prepared by employing this method have controlled properties. The electrospun polymer membranes consist of thin fibers of micron/sub-micron diameters with high specific surface area. The interlaying of fibers generates large porosity with fully interconnected pore structure that facilitates easy transport of ions, and serves as good host matrices for GPEs. Earlier electrochemical studies of PEs based on electrospun membranes of PVdF [8], P(VdF-*co*-HFP)[9,14], PAN [15] and P(VdF-*co*-HFP)/PAN blend [5] have demonstrated their potential application in lithium ion batteries.

Among these host polymers, PAN based electrolytes have shown interesting characteristics like high room temperature ionic conductivity, thermal stability, resistance to oxidative degradation, and good compatibility with the lithium electrodes, which minimize dendrite growth during the charging/discharging process of LIBs [16]. It is reported that the CN groups in PAN could interact with -CO groups of the liquid electrolytes such as propylene carbonate (PC), ethylene carbonate (EC) etc., as well with lithium ions [17]. Many groups demonstrated PAN based GPE prepared by phase inversion method and its electrolyte behavior [17,18]. It is found that PAN provides rigidity and other characteristics to the PEs with augmented lithium ion conduction; however, PAN-based electrolytes have undesirable effects such as liquid extraction from the gel, which results decrease in ionic conductivity for the PEs upon long term storage. Also the porous PAN membranes are very

brittle for the reason that the interaction of adjacent cyanide groups increases the resistance of interior rotation of the main chain and thus decreases the flexibility of the polymer chain [19]. It is reported that these drawback have been overcome by blending PAN with other polymers [5].

PMMA is one of the host polymers previously used in plasticized PEs, which was first reported by Iijima et al. [20] and more recently by Bohnke et al. [10]. Appetecchi et al. [21] studied the kinetics and stability of the lithium electrode in PMMA-based gel electrolytes. PMMA is a common thermoplastic polymer with well-known chemistry. Its amorphous structure is beneficial to ionic conduction and PMMA-based gel electrolytes have shown excellent interfacial stability towards lithium metal. The pendant -$COOCH_3$ is not likely to crystallize around Li^+ as PEO does. PMMA based PEs exhibit high electrolyte uptake, ionic conductivity and good electrochemical stability [22]. Unlike PAN, PMMA has ability to make chemical cross-linking, which will remarkably increase the mechanical strength and the electrolyte solution retention ability of the PE [23,24]. Also it has been reported that gel electrolytes based on cross-linked PMMA can suppress lithium dendrite formation [23].

Polystyrene (PS) is an amorphous polymer having higher T_g (100 $^{\circ}$C) and good thermal stability. Only few reports are there on electrochemical properties of PS and in most cases the material was used in blends with other polymer to provide toughness to the blend [24]. It is well known that, at higher temperatures, the backbone of PS start to slide past each other. This makes PS flexible and stretchable. This quality is coupled with the strength of PAN to develop a tough yet stronger membrane. The aromatic ring in PS also disallows a certain extent of crystallization, which will be useful to enhance the easy transportation of Li^+ ions. This means, the resultant polymer blended membrane can be expected to have more flexibility and ionic conductivity at room temperature.

The present study, reporting microporous membranes based on multi component polymer blend have been prepared for the first time by electrospinning process and the membrane properties as well as the electrochemical properties of the GPEs based on them are evaluated. Homogeneous blend of the polymers PAN, PMMA and PS as matrix polymer for the preparation of porous membranes to exploit the beneficial characteristics of individual polymers. PAN and PMMA are chosen, because it is expected that an uptake of the electrolyte solution may result in swelling or gelation of polymer rather than dissolution. PAN also would contribute to the mechanical stability of the membrane even after soaking in electrolyte solution. PS is selected to make an amorphous path for the easy penetration of Li^+ ions and impart the toughness to the membrane. The porous membrane is prepared by electrospinning method, which is shown to be effective for producing highly porous membranes with good flexibility and mechanical strength [10]. GPEs are prepared by activating them with liquid electrolyte; 1 M lithium hexafluorophosphate ($LiPF_6$) in ethylene carbonate (EC)/diethyl carbonate (DEC). Temperature dependent ionic conductivity and electrochemical properties of the GPEs are evaluated in the process of testing their suitability for application as electrolytes in lithium ion batteries and the results are also compared.

2. Experimental

2.1. Preparation of electrospun PAN–PMMA–PS blend membranes

PAN (M_W 150,000 Sigma Aldrich), PMMA (M_W 120,000, Sigma Aldrich) and PS (M_W 2,000,000, Sigma Aldrich) were vacuum dried at 60 °C for 6 h before use. The solvent *N*,*N*-dimethylformamide (DMF) (Aldrich) was used as received. Fibrous membranes were prepared by the typical electrospinning method at room temperature, as described in previous publications [1,2]. 16% solution of varying content (wt.%) of PAN, PMMA, and PS were dissolved in *N*,*N*-dimethylfomamide (DMF) to get a uniformly blended solution. The resulting solution was degassed for 15 min to get the clear solution. Required quantity of blend solutions were electrospun at ambient atmosphere using a syringe infusion/withdrawal pump (KD Scientific, Model-210). The as spun fibers in the form of nonwoven membrane were collected on a grounded, aluminum drum wrapped with a thin aluminum foil, rotating at specific speed. The essential electrospinning parameters were as follows: applied voltage 16–20 kV (depends on the polymer composition), distance between the tip of the spinneret and collector 20 cm, needle size 0.6 mm, solution feed rate 0.2 ml min^{-1} and collector drum rotation speed 150 rpm. The tailor made blend membrane thickness was carefully controlled during spinning. Electrospun membranes of average thickness 120 μm were collected and dried at room temperature on the drum for 6 h to prevent the shrinking of fibers and then vacuum dried at 60 °C for 12 h before further use. The resulting fibrous blend polymer membranes were represented as BPM-01 (80:10:10), BPM-02 (90:05:05), BPM-03 (90:10:00) and BPM-04 (90:0:10) respectively with polymer composition as PAN:PMMA:PS to highlight their respective composition. Left over blended mixture was solvent casted onto a glass plate using a doctor blade technique and left to dry for 24 h at room temperature and finally vacuum dried at 60 °C for 12 h before tests.

2.2. Characterization of electrospun PAN–PMMA–PS blend membranes

The fiber morphology was recorded with high resolution field-emission scanning electron microscope (FE-SEM: Jeol JSM7600F) at an accelerating voltage of 5 kV. The average fiber diameter (AFD) was estimated based on the micrographs taken at the higher magnification. About 250 fibers were investigated to calculate AFD. The porosity (*P*) was determined by immersing the dry membrane in *n*-butanol for 1 h. Following relation was used to calculate *P*:

$$P\ (\%) = \frac{M_{BuOH}/\rho_{BuOH}}{M_{BuOH}/\rho_{BuOH} + M_m/\rho_P} \times 100 \qquad (1)$$

where M_m is the mass of the dry membrane, M_{BuOH} is the mass of *n*-butanol absorbed, ρ_{BuOH} and ρ_p are the densities of *n*-butanol and polymer, respectively [17].

Thermal properties and crystalline properties of the polymer blend were studied on the solvent cast membranes. Differential scanning calorimetry (DSC: 2950 TA Instruments) at a heating rate of 10 °C min^{-1} under N_2 atmosphere from room temperature to 350 °C and thermo gravimetric analysis (TGA: Q500 TA Instruments) at a heating rate of 10 °C min^{-1}

from room temperature to 775°C under N_2 atmosphere was studied. X-ray diffraction (XRD: Shimadzu Thin film) studies were used to identify the crystallographic structure of the polymer blend.

2.3. Electrochemical evaluation

GPEs based on blend membranes were prepared by soaking a circular piece of the membrane (diameter ~2 cm^2) in the liquid electrolyte, 1 M $LiPF_6$ in EC/DEC (1:1, v/v) (Charslton Technologies Pvt. Ltd.). The resulting GPEs were represented as GPE-01 (80:10:10), GPE-02 (90:05:05), GPE-03 (90:10:00) and GPE-04 (90:0:10) respectively with polymer composition as PAN:PMMA:PS. $LiPF_6$ in mixed carbonate solvents were selected for the study, because this electrolyte is generally employing in commercial LIBs. The electrolyte uptake (δ) was calculated using the relation:

$$\delta\ (\%) = \frac{M - M_0}{M_0} \times 100 \qquad (2)$$

where M_0 is the mass of the dry membrane and M is the mass of the membrane after soaking with the electrolyte. The weight of the wetted membrane was determined at different soaking intervals, and taking care to remove the excess electrolyte remaining on the surface of the membrane by wiping softly with a tissue paper.

The ionic conductivity of the GPEs was measured by the AC impedance method using stainless steel (SS) Swagelok® cells with frequency analyzer using Solartron 1470E and SI 1255B Impedance/gain-phase analyzer coupled with a potentiostat over the temperature range from 0 to 60°C. The electrolyte sample was sandwiched between two SS electrodes and the impedance measurements were performed at an amplitude of 20 mV over the frequency range 10 mHz to 1 MHz. The cell was kept at each measuring temperature for a minimum of 30 min to ensure thermal equilibration of the sample at the temperature before measurement. From the porosity and conductivity measurements, tortuosity of the membranes was calculated from the following relationship:

$$T = \left(\frac{\sigma_0}{\sigma} \times P\right)^{1/2} \qquad (3)$$

where σ_0 and σ are the conductivities of the neat liquid electrolyte and the PE, respectively, and P is the porosity of the membrane. The time dependant interfacial resistance (R_f) between the GPE and lithium metal electrode was measured at room temperature by the impedance response of Li/GPE/Li cells over the frequency range 10 mHz to 1 MHz at an amplitude of 20 mV.

Two-electrode lithium prototype coin cells were fabricated by placing the GPE between lithium metal anode (~300 μm thick) and lithium manganese oxide ($LiMn_2O_4$) cathode. The composite cathode was prepared by mixing 80 wt.% of active material ($LiMn_2O_4$, Merck KGaA, Germany), 10 wt.% of conducting additive (Super P Li carbon) and 10 wt.% of PVdF binder (Kynar 2801) using *N*-methyl pyrrolidinone (NMP) as solvent for the binder to form the slurry. The resulting slurry was coated on to Al foil (~20 μm thick) using doctor blade

technique and subsequently dried in the oven at 70°C. Finally the composite electrode was pressed between stainless steel twin rollers and punched in to circular discs of 16 mm diameter. Before the cell assembly, composite cathode was dried in a vacuum oven at 80°C for 12 h to remove the residual solvent traces, if any. The test cells, Li/GPE/$LiMn_2O_4$ were fabricated in CR2016 coin cell. The electrochemical tests of the Li/GPE/$LiMn_2O_4$ cells were conducted in an automatic galvanostatic charge–discharge unit, battery cycler (BTS XWJ, Neware Tech. Co.), between 3.5 and 4.3 V at 25°C at a current rate of 0.1 C. The activation of electrospun membrane to prepare GPE and the fabrication of test cells were carried out in an argon-filled glove box with oxygen and moisture level <0.1 ppm.

3. Results and discussion

3.1. Membrane morphology

FE-SEM images of PAN–PMMA–PS blend membranes prepared with different compositional ratio reveal the effect of PMMA/PS content on morphology of the fibers and are presented in Fig. 1. FE-SEM images show the membranes are made up of a network of interlaid and straight fibers. It is observed that the fiber morphology of the electrospun PAN–PMMA–PS membranes largely depends on the amount of PMMA and PS in the blend [18,19]. FE-SEM images are giving the vivid information on the presence of well interconnected multi fibrous layers and interstices with ultra fine and fully interconnected pore structure between the fibers. The fibers appear to be uniform in composition without having any microphase separation which shows the compatibility of PAN, PMMA and PS, however, with increase of PMMA/PS content irregularities and nonuniformities are observed. The amount of DMF that remains on the surface of the fiber after electrospinning can partially dissolve and make it amorphous. The residual solvent molecules also help to form smaller pore size due to the formation of relatively large number of cross links [18].

The AFD of fiber obtained for different samples are presented in Table 1. Morphology of the membrane prepared with tri-polymer blend of PAN, PMMA and PS (BPM-01 and BPM-02) is not uniform as bi-polymer blend of PAN with PMMA or PS (BPM-03 and BPM-04). It is found that the AFD is higher for the membranes that contain both PMMA and PS. This may due to the synergic rheological effect of PMMA and PS on the viscosity of the blend solution. The average fiber diameter significantly varied with polymer components and its amount in the blend solution. It is observed that the AFD is higher with higher PS content. This can be attributed to the higher viscosity of PS due to the bulky side group in its chain structure which disallows sliding of the chains from each other, even in the blend solution.

The membrane prepared with the blend solution of PAN–PMMA (BPM-03) has more uniform and narrower distribution of the fiber diameter as compared to the other membranes. The larger diameter of the fiber in membranes with higher content of PMMA and PS can be attributed to the substantial increase in the viscosity that results from the high viscosity of PMMA and PS. Despite the use of a lower polymer concentration (16%), the viscosity of the electrospinning polymer solution is high that affects the ejection of a larger fluid jet from the needle and a consequent deposition of fibers with a larger diameter. All four samples exhibit long and straight fibrous morphology, with an average fiber diameter

from 620 to 950 nm. An order for the decrease of AFD of membranes can be put as: BPM-01 (950) > BPM-02 (887) > BPM-04 (640) > BPM-03 (620). From the FE-SEM images it can be seen that the interlaying of the fibers generates the highly porous fibrous structure for the electrospun membranes, which arises due to the processing parameters employed.

It is well known that the spinning parameters influencing the morphology of electrospun fibrous membranes are solution concentration, solution feed rate, bore size of the needle, distance between the tip of the needle and the collector, rotation speed of the collector, applied voltage, dielectric constant and viscosity of the dope solution. In this study, the first five factors in the above list have been kept as a constant while electrospinning. So it may not be the reasons for the morphological differences. Upon that we envisage the following reasons, the varying content of PMMA and PS changes the dielectric constant of the blend solution and the applied voltage is varied accordingly from 16 to 20 kV to get the uniform fibers. The solution having lower viscosity and higher dielectric constant easily formed Taylor cone at the tip of the needle and caused formation of fibers with lower diameter.

3.2. Thermal properties and crystallinity of the polymer blend

To authenticate the miscibility of component polymers in polymer blends, DSC measurements are employed. Fig. 2 shows the DSC thermograms of PAN–PMMA–PS polymer blends with varying content of PAN, PMMA and PS. All the samples exhibit a weak glass transition and a relatively large and sharp endothermic peak. Table 1 presents the thermal properties of the polymer blends obtained from DSC measurements. PAN–PMMA–PS polymer blends show a sharp melting endotherm ~300°C which is lower than the T_m of pristine PAN. The lower T_m reflects the decrease in crystallinity of PAN in the PAN–PMMA–PS blend. The presence of PS and PMMA in the blend impedes the crystallization of PAN and retains the amorphous domains. The absence of sharp glass transition and any additional endothermic peak for PAN–PMMA–PS blends confirm the miscibility of PAN with PMMA and PS in the polymer blends. The sharp exothermic peak can be attributed to the nucleophilic attack at the nitrile group followed by instantaneous cyclization reaction to an extended conjugated structure, which is exothermic in nature [25]. The heat of fusion (ΔH) of the samples varies with the amount of PMMA and PS in the blend. A decrease in ΔH is observed with increasing content of PMMA and PS. The ΔH values (J g^{-1}) from the DSC data follows the order BPM-01 (390) < BPM-02 (396) < BPM-03 (422) < BPM-04 (435) < PAN (481). The difference in crystallinity arises due to the inhibition of crystallization of PAN molecules by the presence of amorphous PMMA and PS in the polymer blend during the solidification process, which reduces the volume fraction of the crystalline phase in the fiber [26]. By the blending of PMMA and PS with PAN, melting point is slightly lowered, though there is a considerable decrease of melting enthalpy, which corresponds to 9.5–17.7% of PAN. This observation confirms that the blending of PAN with PMMA and PS inhibits the crystallization process of the polymer. It increases the amorphous regions in the polymer, which is beneficial for the purpose of achieving a higher electrolyte uptake and ionic conductivity. Consequently with a decrease in the melting enthalpy, decrease in the melting points of these polymer bends is expected. The melting temperature is 300, 299, 296 and 295°C respectively for BPM-02, BPM-03, BPM-01 and BPM-04, which is in the reverse order of melting enthalpy. This again confirms with the TGA studies, that the decomposition

temperature of these blends is in the same order as its melting temperature observed in DSC studies.

The thermal stability of the PAN–PMMA–PS polymer blend is determined by TGA under N_2 atmosphere from room temperature to 775°C at a heating rate of 10°C min^{-1}. The obtained result is shown in Fig. 3. It can be seen from Fig. 3 that the polymer blend is stable up to 295 ± 5°C. The decomposition temperature of the blends is in the order of BPM-02 (297.6) > BPM-03 (293.2) > BPM01 (288.7) > BPM-04 (285.8). At 450°C the polymer blend shows a weight loss of 44.8, 47.7, 50.3 and 52.5% was observed respectively for BPM-02, BPM-03, BPM-01 and BPM-04. From 450 to 470°C a weight loss of 13.8 and 6.4% was observed for the BPM-01 and BPM-04 respectively, while BPM-02 and BPM-03 showed only 1.5–2.8% weight loss. The char yield at 775°C is 33.8, 35.7, 41.9 and 42.8% respectively for BPM-04, BPM-01, BPM-03 and BPM-02. Compared to BPM-01, the high char yield of BPM-02 is attributed to the higher PAN content (90 wt.%) in the blend.

The X-ray diffraction was employed to analyze the crystallization behaviors of PAN–PMMA–PS polymer blends. Fig. 4 shows the XRD patterns of pristine PAN, PMMA, PS and its blends BPM-01, BPM-02 and BPM-04. It is found that only an amorphous peak at about 2θ value ~20 exists in the full range of 2θ. In the case of pristine PAN the spectrum shows a sharp intense peak centered at 17.7 and a weak diffraction peak at 29.6 is the characteristics peaks of plane of PAN crystallite. The first peak corresponding to the lateral repeating distance or Bragg spacing is identified as (1 0 0) hexagonal lattice. The weak diffraction peak corresponds to the second order diffraction of the first peak [27]. The relatively wider diffraction peak for PMMA and PS reflects the amorphous nature of the polymers. Compared to diffraction peak of pristine PAN, a peak shift of 1.2° to the lower 2θ side, lowering and widening of the diffraction intensity of the peak is observed when PAN is blended with PMMA and PS. This clearly indicates a decrease in the crystallinity leading to reduce the energy barrier to the chain movement, which confirms the reduction of crystallinity observed in DSC studies. The d-spacing of peak (2θ = 17.7) for pristine PAN, BPM-02 and BPM-01 is 5.75, 6.92, 7.52 Å corresponding to the (1 0 0) diffraction of the hexagonal lattice. For PAN–PMMA–PS blend polymer samples, d-spacings and sizes of apparent crystallite are increased, while the degree of crystallinity is decreased with increasing PMMA and PS content. Therefore, the lower crystallinity of the polymer blend is expected to contribute high ionic conductivity to the PAN–PMMA–PS polymer blend based GPE.

3.3. Porosity, electrolyte uptake and electrolyte retention

Porosity is the one of the important parameters of PEs based on electrospun membranes in LIBs. The interlaying of the fibers generates porous structure in the electrospun membrane. Porosity of the prepared membranes is determined by *n*-butanol uptake method. The *n*-butanol does not interact with the membrane; it rather penetrates the pores and occupies all the available pores, and thus gives a measure of the total pore volume in the material. The porosity of the membranes prepared varies in the narrow range 80–84% showing slight increase with PMMA/PS content. This difference in porosity is attributed as the loose packing of fibers in the layers of the membrane and average fiber diameter of

the membrane. The presence of a large number of interconnected pore structures from the FE-SEM image is evidence.

The electrolyte uptake of the porous membrane is greatly dependent on the porosity and pore structure of the membranes. Fig. 5 shows the electrolyte uptake (1 M $LiPF_6$ in EC/DEC) behavior of the electrospun PAN–PMMA–PS fibrous membranes. The data is obtained by soaking the membranes in the liquid electrolyte for a period of 1 h. The blend fibrous membrane BPM-01 shows an electrolyte uptake of about 500% within 2 min, while the BPM-02 and BPM-04 is only 480 and 472% respectively. After 1 h the electrolyte uptake reaches up to 685, 662, 673 and 650% respectively for BPM-01, BPM-02, BPM-03 and BPM-04. The absorption of the large quantities of liquid electrolyte by the blend membranes results from the high porosity of the membranes and the high amorphous content of the polymer blends. Thus, the electrolyte uptake of ~650% achieved in this study is higher than that reported earlier [28] for a PAN membrane of ~86% porosity. The difference in electrolyte uptake is due to not only the difference in porosity values of membranes but also the ability for partial swelling of the fibers which will hold more electrolytes. According to Kataoka et al. [29] there are two distinct steps for liquid electrolytes uptake in porous gel polymer membranes. Firstly, the liquid electrolyte occupies pore spaces of the membrane and then those electrolytes in the pores penetrate and swell the polymer chains to form the gel. In the case of membranes with higher PMMA/PS content the density of the membrane is less due to the loose packing of the fibers. High amorphous content also enhances degree of swelling of the fibers and the large number of smaller pores adds up to high pore volume and pore surface area. Both the lower density, higher amorphous content and high pore surface area facilitate the easy swelling of more polymer chains and it leads to the higher level of electrolyte uptake of the electrospun membrane containing higher PMMA/PS content. It is observed that after soaking in 1 M $LiPF_6$ in EC/DEC electrolyte solution, all the membranes retained their fibrous nature [28]. The fully interconnected pore structure makes fast penetration of the liquid into the membrane possible, and hence the uptake process is stabilized within the initial 15 min, however, it must be taken to note that the polymer blends BPM-02 and BPM-04 have a lower uptake than the other two. One speculation could be due to the steric hindrance of the benzene ring that PS has. This hindrance could retard/prevent the penetration of electrolyte to the core of the fibers. The tortuosity of the membranes is calculated from the porosity and the ionic conductivity and listed in Table 1. It is observed that, the tortuosity of PAN–PMMA–PS blend membranes greatly depends on porosity rather than ionic conductivity.

3.4. Ionic conductivity

Fig. 6 shows the temperature dependant ionic conductivity of GPE based on electrospun blend polymer membranes containing different PAN–PMMA–PS content on the heating cycle from 0 to 60 °C for 1 M $LiPF_6$ in EC/DEC. The behavior is similar to the liquid electrolyte. The conductivity range is between 10^{-4} and 10^{-2} S cm^{-1}, and in all the explored temperatures the maximum conductivity corresponds to the GPE-01. This can be attributed to the lower crystallinity of the membrane due to the higher content of PMMA and PS in the polymer blend. The ionic conductivity of the GPEs is 10^{-3} S cm^{-1} for all the samples at room temperature. Comparing the ionic conductivity of BPM-02, BPM-03 and BPM-04, which contain 90% PAN, BPM-03 seems to slightly outperform. This indicates

that PS in the blend does not significantly affect the ionic conductivity of the membrane. This can be attributed to the lower dielectric constant (2.5) and rigid nature of the PS molecules, compared to the PMMA (dielectric constant 3.9). It is observed that the values of ionic conductivity seems to correlate to the electrolyte uptake of the polymer blend with the highest uptake (BPM-01 and BPM-03) having a correspondingly higher ionic conductivity across all temperature ranges studied here. This might also indicate that the increased ionic conductivity is less due to the polymer host but more due to the electrolyte content in the GPE.

The 1 M $LiPF_6$ in EC/DEC is reported to have an ionic conductivity of 7 x 10^{-3} S cm^{-1} at 25 °C [30]. The extent of conductivity loss for the electrolyte due to the use of electrospun membrane in the PE is thus seen to be very low (i.e. a loss factor of ~0.4, compared with the conductivity of 3.9 x 10^{-3} S cm^{-1} for the PE at 25 °C). The lower ionic conductivity of GPE compared to its liquid electrolyte may due to the slower conduction path in the swollen polymer phase along with the tortuous path taken by the ions in the membrane pores. In summary it is found that the fully interconnected pore structure of the electrospun membrane used in the present study allows the easier passage of ions between the electrodes.

As shown in Fig. 6, the ionic conductivity is found to increase with the temperature. The $\log \sigma$ vs. $1/T$ curves for all the GPEs show that within the temperature range 0–60 °C the Arrhenius plots are not very linear, it suggests that the conductivity of PAN–PMMA–PS blend based GPE does not obey the simple Arrhenius equation [$\sigma = \sigma_0 \exp(-E_a/RT)$]. So that activation energy for ionic conduction E_a can be obtained using the Vogel–Tamman–Fulcher (VTF) model { $\sigma = \sigma_0 T^{-1/2} \exp[-E_a/R(T - T_0)]$} often used for the treatment of the curved Arrhenius plots. This behavior is characteristic of the amorphous polymeric electrolytes [31], which follows free-volume model [32]. From the linear and parallel curves of all the samples suggested that given the low difference in the activation energies and porosity of different samples, the variation of average pore size does not influence the activation energy for ionic conduction [33].

3.5. Electrochemical properties

3.5.1. Interfacial resistance

The formation of a stable solid electrolyte interface on the lithium metal that can conduct Li^+ ions freely and at the same time prevent any undesired interaction between the electrolyte components and lithium leading to dendrite formation is essential for attaining good cycle performance. Mobility of lithium ions in the GPE is estimated by AC impedance measurements using Li/GPE/Li symmetric cell. The initial impedance behavior of GPE based on PAN–PMMA–PS blend membranes with 1 M $LiPF_6$ in EC/DEC on lithium metal at ambient temperature is shown in Fig. 7. The spectrum exhibit a single semi-circle over the whole frequency range typical of the electrolytes with contributions from bulk electrolyte resistance (R_b) and electrode/electrolyte interfacial resistance (R_f). Such pattern is generally shown by liquid/gel electrolytes that have high ionic conductivity. (i.e. low R_b value). All the samples display similar curvature but the diameter of the semi circle varies from sample to sample suggesting different kinetics [34]. The R_b values are low and lies in the range 3–6 Ω for the GPEs. The values are in agreement with low R_b observed for these electrolytes in

SS/GPE/SS cells as described above in Section 3.4, and this supports high ionic conductivities of the GPEs. This again confirms that the fully interconnected porous and fibrous structure of electrospun blend polymer membranes can function as an efficient ion transport media between the electrodes. The initial interfacial resistance R_i is minimum for GPE-02. The R_i values are 303, 254, 406 and 522Ω respectively for GPE-01, GPE-02, GPE-03 and GPE-04. The Ri of GPEs based on tri-polymer blends is 25–52% less when compared with binary polymer blends. This may be due to the morphological difference of the membranes and the synergic effect of PMMA and PS in the tri-polymer blend.

The variation of interfacial impedance of lithium metal electrode in contact with GPE has been analyzed under prolonged exposure at room temperature and is presented in Fig. 8. It is found that the interfacial resistance of all GPEs increases with storage time. The observed initial increase in the impedance implies that the lithium electrode is passivated with time due to the reactivity of the lithium electrode and the polymer electrolyte. Given the intrinsic stability of the polymer backbone, one might speculate that the lithium electrode reacts with carbonate based electrolytes. Aprotic solvents such as EC and DEC are well known for forming a passivating layer on lithium metal [35]. The R_f values shows that the interfacial resistance is less for the GPE based on tri-polymer blends even after 5 days storage. It is found that after 4 days of storage the interfacial resistance of the GPE reached to its maximum and then starts to decrease. This implies the stabilization of the passivating layer at the interface of lithium metal and GPE. The early stabilization of passive film indicates that the immobilized electrolyte within the three dimensional network of fibers in electrospun blend membranes is well encapsulated in the matrix polymer due to the good compatibility between polymer blend and aprotic solvent, which reduces the reactivity towards lithium metal as well as noted that the tri-polymer blends are better than the binary polymer blends. GPE-02 having higher PAN content (compared to GPE-01) behaves significantly better than all the other blends. GPE-02 not only shows a lower interfacial resistance but also a lower rate of increase in resistance. This can be attributed to the better interfacial stability offered by higher level of PAN content (90%) in the tri-polymer blend [28]. After four days of storage all the GPEs showed higher interfacial resistance compared to its Ri, for instance, 100, 60, 41 and 64% increase is noted for GPE-01, GPE-02, GPE-03 and GPE-04, respectively with respect to their initial interfacial resistance.

3.5.2. Evaluation in Li/$LiMn_2O_4$ cell

Among various cathode materials, $LiMn_2O_4$ is the most widely used in commercial LIBs due to its, low cost, environmental sustainability, high energy density, high operating voltage and good electrochemical performance with charge cutoff voltage 4.5 V. Coin cells are assembled by sandwiching GPE between Li metal anode and $LiMn_2O_4$ composite cathode film. The electrochemical performance of the cells is evaluated by galvanostatic cycling under constant current of 0.1 C between 3.5 and 4.3 V. Fig. 9 shows the first charge – discharge profile (first cycle) of the Li/$LiMn_2O_4$ coin cells using PAN – PMMA – PS blend based GPE at 25 ◦C. Relatively high cathode utilization corresponding to 79.0 – 82.4% of theoretical capacity is achieved. The cell based on the polymer electrolyte with GPE-01 delivers initial discharge capacity of 122 mAh g^{-1}. All other cells show a discharge capacity 3.3 – 4.9% lower as compared to cell with GPE-01. The

difference in discharge capacity is probably due to the difference in the utilization of active material. The GPE-01 shows the highest porosity and contains the largest amount of liquid electrolyte, and hence more liquid electrolyte can diffuse from the polymer electrolyte to the composite cathode, which leads to higher utilization of the active material. The difference in ionic conductivity of the GPEs also may affect the discharge property. However, the experimental capacity of all the cells is close to the theoretical capacity of $LiMn_2O_4$ (148 mAh g^{-1}). The better discharge capacity profile has been observed for the test cells comprising GPE-01 with higher PMMA content when compared to rest of the GPEs investigated. This improved performance is attributed to the higher amorphous content, electrolyte uptake and ionic conductivity of GPE-01. The discharge capacity versus cycle number for the cell subjected to 50 cycles is shown in Fig. 10. It is seen that discharge capacity is slightly decreasing with number of cycling. After 50 cycles the cell with GPE-01 retains a discharge capacity of 113 mAh g^{-1}, which is 92.7% of its initial discharge capacity and is 1.2 – 7.8% higher than other cells. These results confirm the excellent efficiency of the PAN – PMMA – PS blend polymer membrane to conduct the ions between electrodes during cycling processes. The decline in the discharge capacity is not significantly pronounced for all the GPEs. This indicates that PAN – PMMA – PS blend tri-polymer membranes have good compatibility with electrodes (as discussed in Section 3.5.1), especially to lithium metal. This fade in capacity is related to the interfacial property between the polymer electrolyte and the electrode. During the cycling, the physical changes in the active materials and the passivation film on the surface of the electrode gradually increase cell internal resistance, which results in the discharge capacity loss with cycling. This evaluation demonstrates the suitability of blend polymer electrolytes based on an electrospun membrane for lithium ion battery applications.

4. Conclusions

The polymer electrolytes based on fibrous PAN–PMMA–PS blend membranes are prepared by electrospinning technique. Fibrous membranes with uniform morphology having average fiber diameter of ~620–950 nm is obtained under the optimized conditions. The thermal stability is found higher for the polymer blends comprising higher PAN content. The crystallinity of the polymer blends are studied by DSC and XRD and the results shows that the component polymers in the blends are miscible. The activation of PEs has been carried out by soaking the membranes in 1 M $LiPF_6$ in EC/DEC. It is worth to mention that, the ionic conductivity is improved by increasing PMMA content. Among the polymer electrolytes prepared, the maximum ionic conductivity is found 3.9 x 10^{-3} S cm^{-1} at 25 °C. All PEs shows good compatibility with lithium metal electrodes. The $Li/LiMn_2O_4$ cell using GPE based on blend polymer membranes delivers an initial discharge capacity of ~120 mAh g^{-1} at 0.1 C with stable cycling properties in room temperature. High electrolyte uptake, high ionic conductivity, stable interfacial properties, and appreciable cycle performance indicate that PEs based on electrospun polymer membranes can be used in future lithium ion batteries.

Acknowledgments

This work was supported by funding from the National Research Foundation, Clean Energy Research Project grant number NRF2009EWT-CERP001-036. The authors are also thankfully acknowledged Prof. J.H. Ahn, N. Shubha, W.F. Mak and H.S.W. Joel for helpful discussion and assistance to finish this work.

References

[1] J. Choi, G. Cheruvally, Y. Kim, J. Kim, J. Manuel, P. Raghavan, J. Ahn, K. Kim, H. Ahn, D. Choi, C. Song, Solid State Ionics 178 (2007) 1235.

[2] G. Appetecchi, F. Croce, J. Hassoun, B. Scrosati, M. Salomon, F. Cassel, J. Power Sources 114 (2003) 105.

[3] M. Watanabe, M. Kanba, H. Matsuda, K. Tsunemi, K. Mizoguchi, E. Tsuchida, I. Shinohara, Die Macromol. Chem. Rapid Commun. 2 (1981) 74.

[4] S. Mitra, A.K. Shukla, S. Sampath, J. Power Sources 101 (2001) 213.

[5] P. Raghavan, X. Zhao, C. Shin, D.H. Baek, J.W. Choi, J. Manuel, M.Y. Heo, J.H. Ahn, C. Nah, J. Power Sources 195 (2010) 6088.

[6] A.M. Stephan, T.P. Kumar, N.G. Renganathan, S. Pitchumani, R. Thirunakaran, N. Muniyandi, J. Power Sources 89 (2000) 80.

[7] S. Ramesh, H.M. Ng, Solid State Ionics 192 (2011) 2.

[8] J. Kim, S. Choi, S. Jo, W. Lee, B. Kim, Electrochim. Acta 50 (2004) 69.

[9] X. Li, G. Cheruvally, J. Kim, J. Choi, J. Ahn, K. Kim, H. Ahn, J. Power Sources 167 (2007) 491.

[10] O. Bohnke, G. Frand, M. Rezrazi, C. Rousselot, C. Truche, Solid State Ionics 66 (1993) 97.

[11] D. Peramunage, D.M. Pasquariello, K.M. Abraham, J. Electrochem. Soc. 142 (1995) 1789.

[12] Z. Wang, Z. Tang, Mater. Chem. Phys. 82 (2003) 16.

[13] J.W. Choi, J.H. Kim, G. Cheruvally, J.H. Ahn, K.W. Kim, H.J. Ahn, J.U. Kim, J. Ind. Eng. Chem. 12 (2006) 939.

[14] P. Raghavan, X. Zhao, J. Manuel, C. Shin, M.Y. Heo, J.H. Ahn, H.S. Ryu, H.J. Ahn, J.P. Noh, G.B. Cho, Mater. Res. Bull. 45 (2010) 362.

[15] S. Choi, J. Kim, S. Jo, W. Lee, Y.R. Kim, J. Electrochem. Soc. 152 (2005) A989.

[16] H. Tsutsumi, A. Matsuo, K. Takase, S. Doi, A. Hisanaga, K. Onimura, T. Oishi, J. Power Sources 90 (2000) 33.

[17] K.M. Abraham, M. Alamgir, J. Electrochem. Soc. 137 (1990) 1657.

[18] H.S. Min, J.M. Ko, D.W. Kim, J. Power Sources 119–121 (2003) 469.

[19] G. Wu, H.Y. Yang, H.Z. Chen, F. Yuan, L.G. Yang, M. Wang, R.J. Fu, Mater. Chem. Phys. 104 (2007) 284.

[20] T. Iijima, Y. Toyoguchi, N. Eda, Denki Kagaku 53 (1985) 619.

[21] G. Appetecchi, F. Croce, B. Scrosati, Electrochim. Acta 40 (1995) 991.

[22] H. Rhoo, H.T. Kim, J.K. Park, T.S. Hwang, Electrochim. Acta 42 (1997) 1571.

[23] T. Tatsuma, M. Taguchi, N. Oyama, Electrochim. Acta 46 (2001) 1201.

[24] F.M. Gray, J.R. MacCallum, C.A. Vincent, Solid State Ionics 18 (1986) 282.

[25] P. Rittigstein, J.M. Torkelson, J. Polym. Sci. B: Polym. Phys. 44 (2006) 2935.

[26] C. Leo, A.K. Thakur, G.V.S. Rao, B.V.R. Chowdari, J. Power Sources 115 (2003) 295.

[27] O.Y. Se, K.B. Kyu, Polymer 38 (1997) 5211.

[28] P. Raghavan, J. Manuel, X. Zhao, D.S. Kim, J.H. Ahn, C. Nah, J. Power Sources 196 (2011) 6742.

[29] H. Kataoka, Y. Saito, T. Sakai, E. Quartarone, P. Mustarelli, J. Phys. Chem. B 104 (2000) 11460.

[30] K. Hayashi, Y. Nemoto, S. Tobishima, J. Yamaki, Electrochim. Acta 44 (1999) 2337.
[31] A.M. Christie, L. Christie, C.A. Vincent, J. Power Sources 74 (1998) 77.
[32] S. Ahmad, T.K. Saxena, S. Ahmad, S.A. Agnihotry, J. Power Sources 159 (2006) 205.
[33] J.Y. Song, C.L. Cheng, Y.Y. Wang, C.C. Wan, J. Electrochem. Soc. 149 (2002) A1230.
[34] C.V.S. Reddy, A.P. Jin, X. Han, Q.Y. Zhu, L.Q. Mai, W. Chen, Electrochem. Commun. 8 (2006) 279.
[35] J. Thevenin, R. Muller, J. Electrochem. Soc. 134 (1987) 273.

List of Figures

List of Table

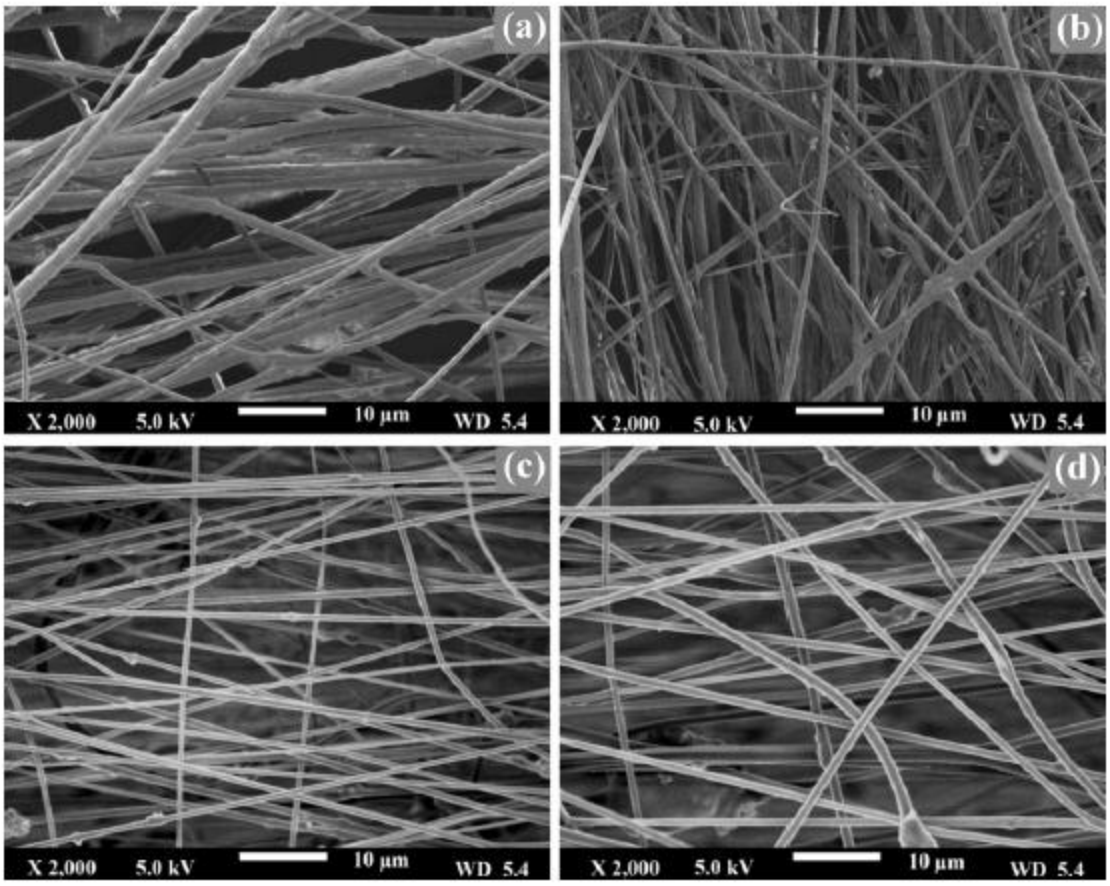
(a)
X 2,000 5.0 kV 10 µm WD 5.4
(b)
X 2,000 5.0 kV 10 µm WD 5.4
(c)
X 2,000 5.0 kV 10 µm WD 5.4
(d)
X 2,000 5.0 kV 10 µm WD 5.4

Figure 1

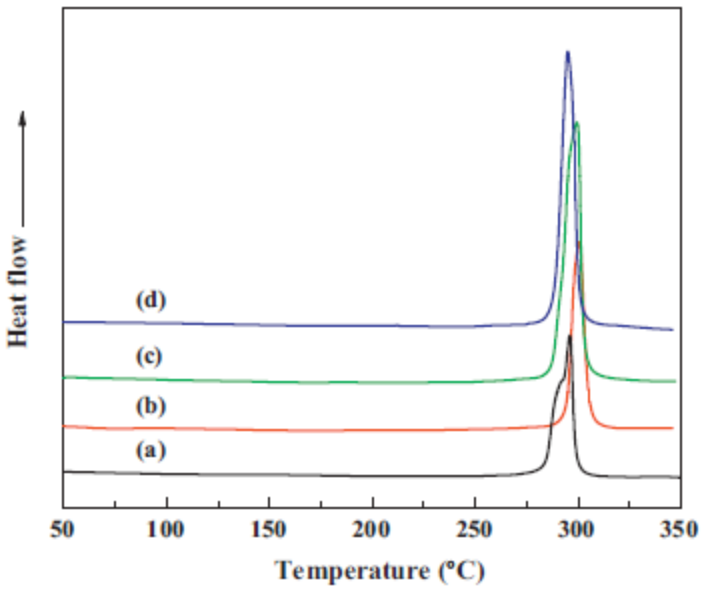

Figure 2

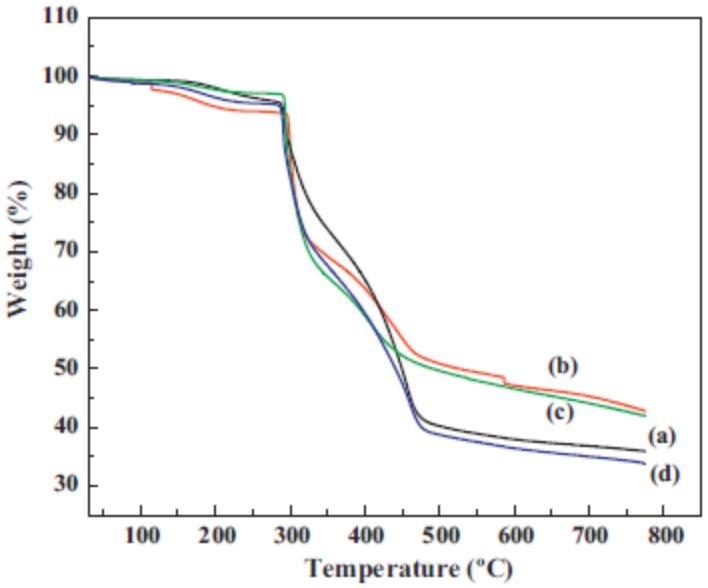
110
100
90
80
70
60
50
40
30
Weight (%)
100
200
300
400
500
600
700
800
Temperature (°C)
(b)
(c)
(a)
(d)

Figure 3

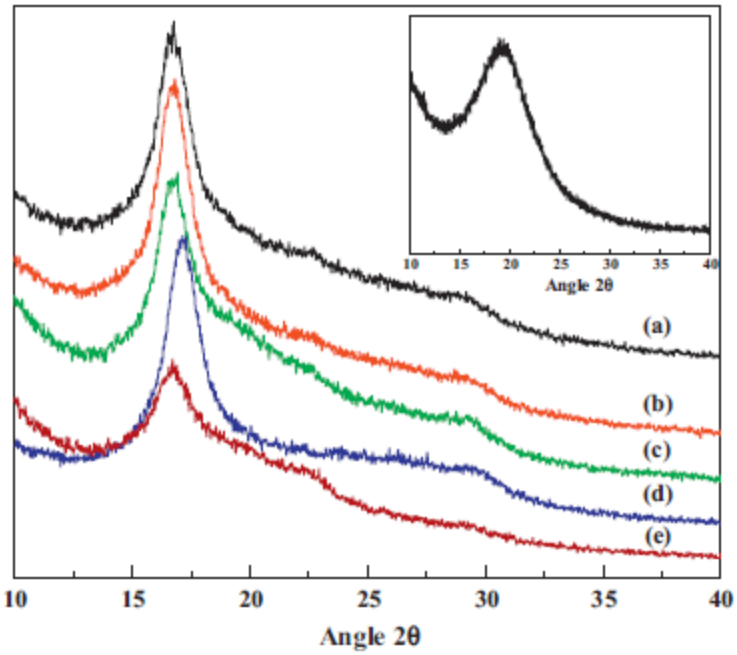

Figure 4

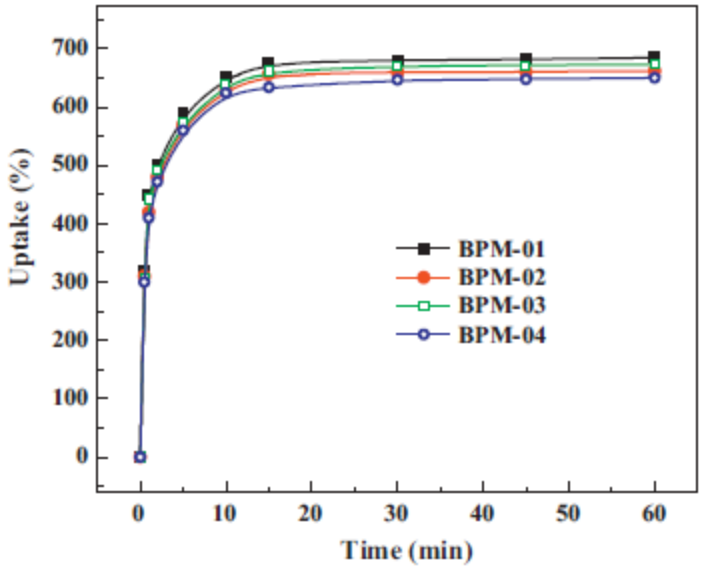
Uptake (%)
700
600
500
400
300
200
100
0
0
10
20
30
40
50
60
Time (min)
BPM-01
BPM-02
BPM-03
BPM-04

Figure 5

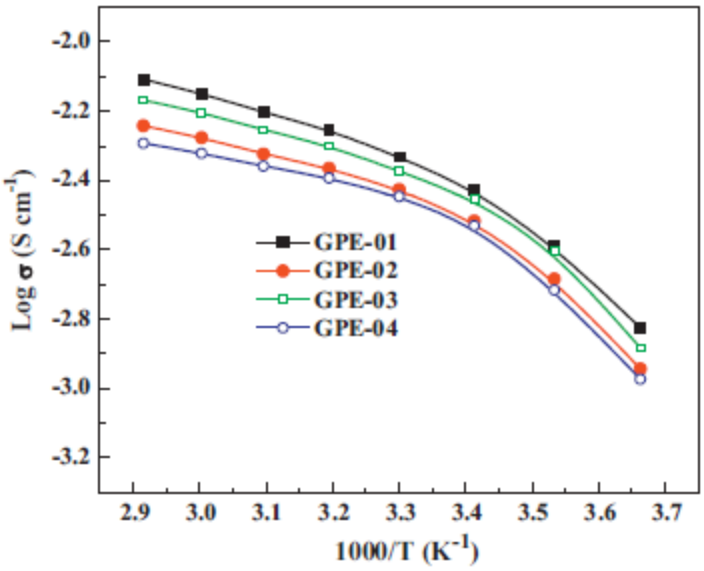
-2.0
-2.2
-2.4
-2.6
-2.8
-3.0
-3.2
Log σ (S cm-1)
2.9
3.0
3.1
3.2
3.3
3.4
3.5
3.6
3.7
1000/T (K-1)
GPE-01
GPE-02
GPE-03
GPE-04

Figure 6

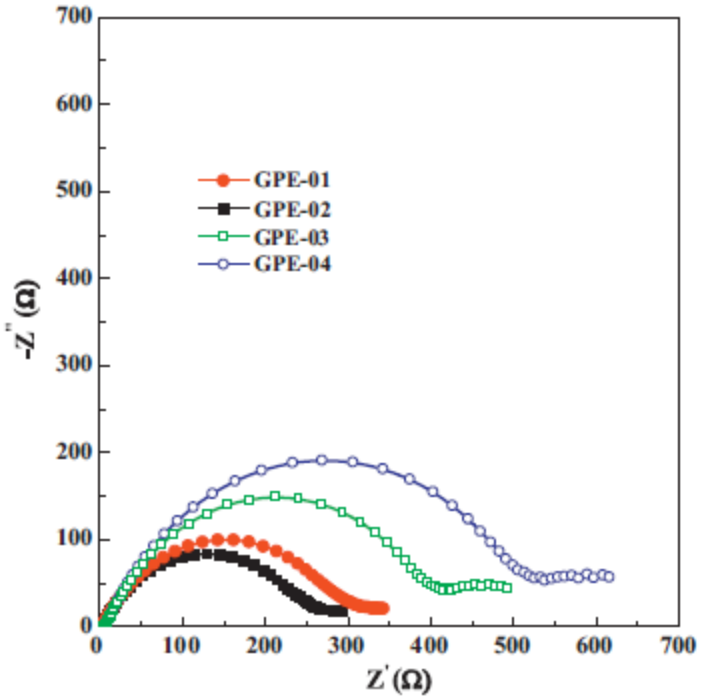

Figure 7

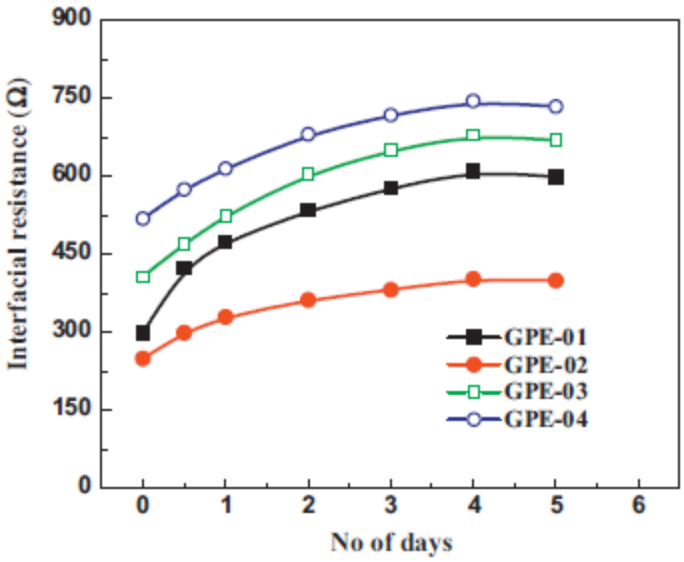
Interfacial resistance (Ω)
900
750
600
450
300
150
0
0
1
2
3
4
5
6
No of days
GPE-01
GPE-02
GPE-03
GPE-04

Figure 8

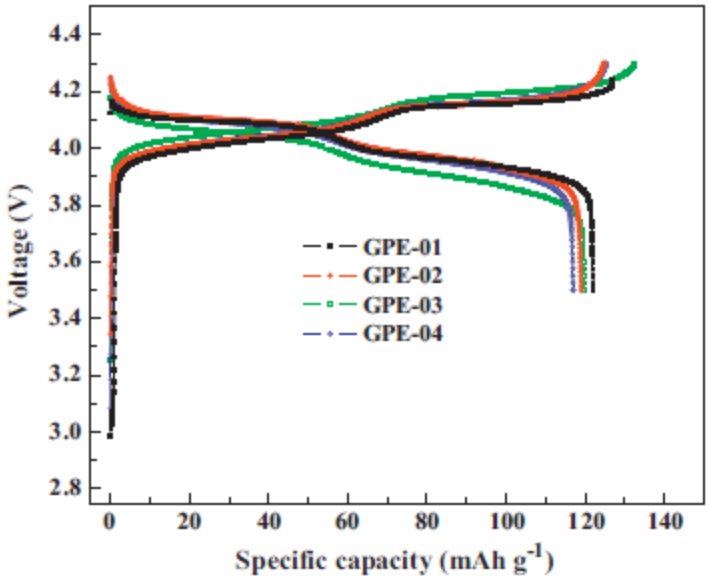
4.4
4.2
4.0
3.8
3.6
3.4
3.2
3.0
2.8
Voltage (V)
0
20
40
60
80
100
120
140
Specific capacity (mAh g-1)
GPE-01
GPE-02
GPE-03
GPE-04

Figure 9

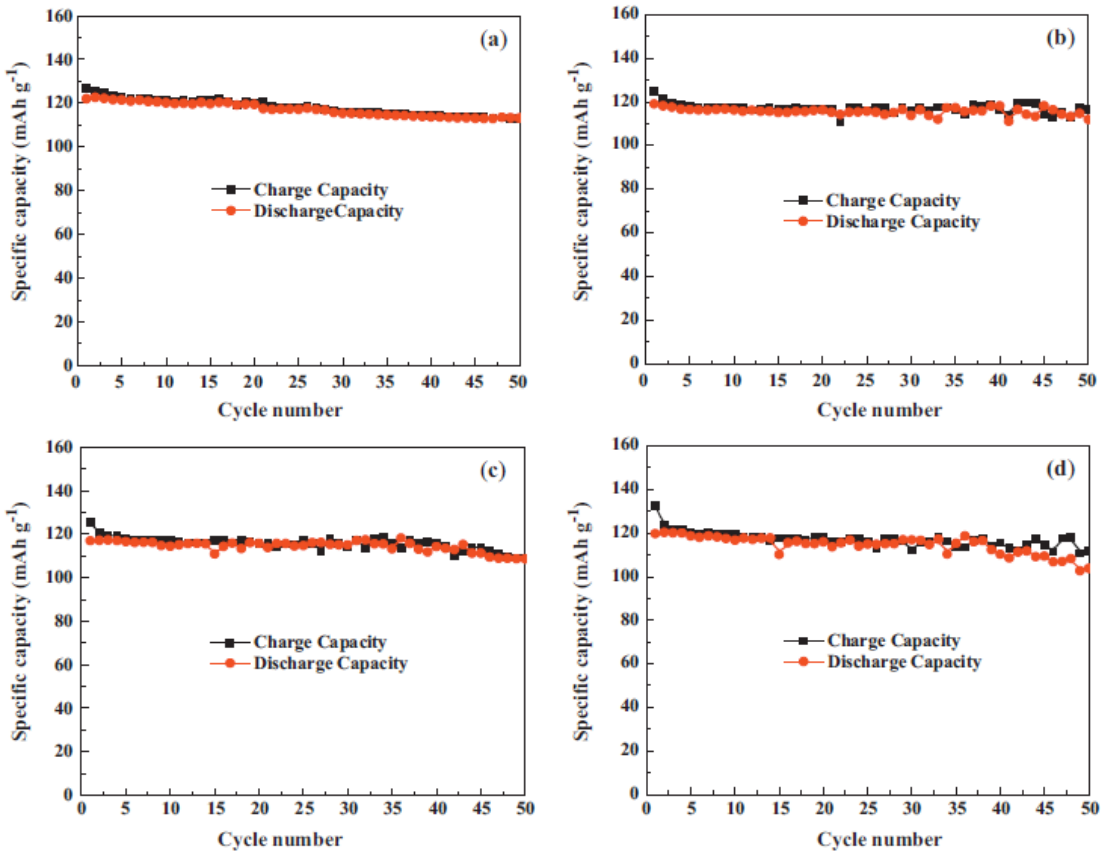
(a)
Charge Capacity
DischargeCapacity
Specific capacity (mAh g-1)
Cycle number
(b)
Charge Capacity
Discharge Capacity
Specific capacity (mAh g-1)
Cycle number
(c)
Charge Capacity
Discharge Capacity
Specific capacity (mAh g-1)
Cycle number
(d)
Charge Capacity
Discharge Capacity
Specific capacity (mAh g-1)
Cycle number

Figure 10

Sample	Melting temperature (°C)	AFD (nm)	Porosity (%)	Uptake (wt.%)	Ionic conductivity ($mS\,cm^{-1}$)	Tortuosity
BPM-01	296	950	84	685	3.9	12.3
BPM-02	300	887	85	661	3.1	13.8
BPM-03	299	620	82	673	3.6	12.6
BPM-04	295	640	80	650	2.7	14.4

Table 1